



# Channel geometry optimization for vertical axis wind turbines in skyscrapers

Seifeddine Kefi<sup>a</sup>, Ajay Joneja<sup>a</sup>, Tim K.T. Tse<sup>b</sup> and Sunwei Li<sup>c</sup>

<sup>a</sup>Dept of IELM, HKUST, Hong Kong; <sup>b</sup>Dept of Civil Engg, HKUST, Hong Kong; <sup>c</sup>Div of Ocean Sci & Tech, Tsinghua University, China

## ABSTRACT

The desire for sustainability and improved air quality has led architects to explore integrating *vertical axis wind turbines* (VAWT) in urban skyscrapers. However, the efficiency of such solutions is sensitive to the geometry of the wind channel. In this paper, we present a general technique for optimization of the wind channel geometry. Using parametric curves to define the profile of the channel, and by quantizing the location of the control points, we propose an experimental design approach to determine near-optimal channel geometry. The solution is further improved by interpolating the performance function so obtained via a statistical tool called kriging. The approach is tested by an experimental study, in which the parameters of the fluid dynamic model are determined by a series of wind tunnel tests.

## KEYWORDS

Sustainable architecture;  
vertical axis wind turbines;  
green buildings

## 1. Introduction

The desire for introduction of clean energy in urban environments has led to some interest in the use of wind power integrated into modern cities. One way to do so is to integrate wind turbines into skyscrapers, as is seen in some recent architectural projects such as the Pearl River Tower in Guangzhou (Figure 1). Obviously we would like to maximize the power output from such a design, which is a function not only of the parameters of the *vertical axis wind turbine* (VAWT), but also on the patterns of prevailing winds, the topography of the surrounding environment, and the shape of the channel in which the VAWT is installed. In this paper, we shall explore how to optimize the shape of the channel when the other controlling factors have been determined. We focus on VAWTs since they are generally better suited to urban environments due to ease of maintenance and lower noise [9]. The approximate power generated by a VAWT's is given by  $P_M = \frac{1}{2} \rho C_p U^3 \frac{\pi d^2}{4}$ , where  $\rho$  is the air density,  $d$  is the turbine diameter,  $U$  is the wind velocity, and  $C_p$  is the capacity factor, which is the ratio of the power generated to the available power, and is governed by the Betz limit to approximately 59% for Newtonian fluids. While VAWTs may be installed in a few different configurations, we will limit this work to in-building duct installations, such as the one used in the Pearl River Tower in Guangzhou as shown in Fig. 1.

Our approach is summarized as follows. We assume that the VAWT is installed in a horizontal channel. The

shape of the channel will be modeled by a parametric surface whose cross-section varies along the direction of the wind (assumed to be normal to the building face). The wind flow is modeled by a fluid dynamic model that considers turbulence in the boundary layer. The model is solved numerically using standard computational fluid dynamics (CFD). However, the solver requires accurate estimates of some parameters, which are estimated by running a wind tunnel experiment on a scaled model. A design of experiments technique is used to experiment with a series of channel shapes. Finally, a statistical interpolation tool is used to interpolate the response function of the experiments, to determine the best possible shape (i.e. the one which gives the maximum velocity of the wind at the contraction point of the channel).

## 2. Background

### 2.1. Wind flow modeling

Modeling for flow in urban environments requires the use of computational fluid dynamic models. In particular, since the air flow in the atmospheric boundary layer (ABL) is turbulent, modified forms of the standard Navier-Stokes equations are required. One commonly used model is the RANS (Reynolds Average Navier Stokes) model, which essentially expresses the flow velocity as an average velocity plus a fluctuation term,  $u_i(t) = \bar{U}_i + u'_i(t)$ , where the subscript  $i$  denotes the coordinate. Similarly, the pressure is expressed as:  $P(t) = \bar{P} + p'(t)$ .

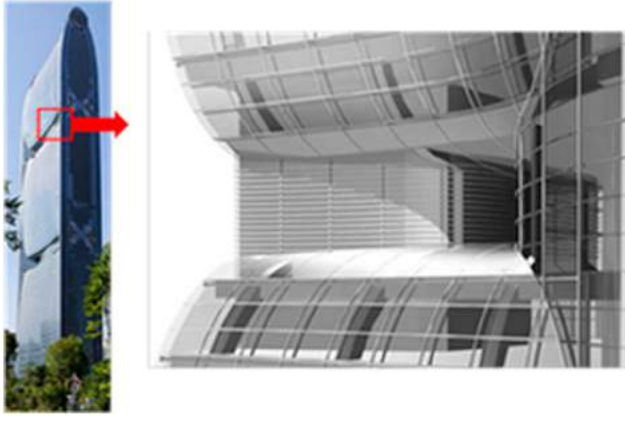


**Figure 1.** Pearl River Tower, Guangzhou; SOM architects [12].

This gives the RANS model for continuity and momentum with the velocity  $\bar{u} = (U, V, W)$  as [10]:

$$\frac{\partial \bar{U}}{\partial x} + \frac{\partial \bar{V}}{\partial y} + \frac{\partial \bar{W}}{\partial z} = 0 \quad (1)$$

$$\frac{D\bar{U}}{Dt} = -\frac{1}{\rho} \frac{\partial \bar{P}}{\partial x} - \frac{\partial \overline{u'u'}}{\partial x} - \frac{\partial \overline{u'v'}}{\partial y} - \frac{\partial \overline{u'w'}}{\partial z} - \nu \nabla^2 \bar{U} \quad (2)$$

$$\frac{D\bar{V}}{Dt} = -\frac{1}{\rho} \frac{\partial \bar{P}}{\partial y} - \frac{\partial \overline{u'v'}}{\partial x} - \frac{\partial \overline{v'v'}}{\partial y} - \frac{\partial \overline{v'w'}}{\partial z} - \nu \nabla^2 \bar{V} \quad (3)$$

$$\frac{D\bar{W}}{Dt} = -\frac{1}{\rho} \frac{\partial \bar{P}}{\partial z} - \frac{\partial \overline{u'w'}}{\partial x} - \frac{\partial \overline{v'w'}}{\partial y} - \frac{\partial \overline{w'w'}}{\partial z} + \nu \nabla^2 \bar{W} \quad (4)$$

Unfortunately, the additional Reynolds stress terms  $\overline{u'_i u'_j}$  imply that this system has ten unknowns in four equations, and therefore is under-constrained. To handle this issue, Kolmogorov [5] suggested modeling the turbulence using two numbers: the turbulent kinetic energy  $k$  and the turbulence dissipation rate  $\varepsilon$ :

$$k = \frac{1}{2} \overline{u'_i u'_i} \quad (5)$$

$$\varepsilon = \nu \overline{\frac{\partial u'_i}{\partial x_j} \left( \frac{\partial u'_i}{\partial x_j} + \frac{\partial u'_j}{\partial x_i} \right)} \quad (6)$$

This led to the development of the standard k- $\varepsilon$  model by Hanjalic and Launder [3]:

$$\frac{\partial \bar{U}_i}{\partial x_i} = 0 \quad (7)$$

$$\frac{D\bar{U}_i}{Dt} = -\frac{1}{\rho} \frac{\partial \bar{P}}{\partial x_i} + \nu \nabla^2 \bar{U}_i \quad (8)$$

$$\begin{aligned} \frac{\partial k}{\partial t} + u_i \frac{\partial k}{\partial x_i} &= \frac{\partial}{\partial x_i} \left( \frac{\nu_T}{C_k} \frac{\partial k}{\partial x_i} \right) \\ &+ \nu_T \left( \frac{\partial \bar{U}_i}{\partial x_j} + \frac{\partial \bar{U}_j}{\partial x_i} \right) \frac{\partial \bar{U}_i}{\partial x_j} - \varepsilon \end{aligned} \quad (9)$$

$$\begin{aligned} \frac{\partial \varepsilon}{\partial t} + u_i \frac{\partial \varepsilon}{\partial x_i} &= \frac{\partial}{\partial x_i} \left( \frac{\nu_T}{C_\varepsilon} \frac{\partial \varepsilon}{\partial x_i} \right) \\ &+ C_{1\varepsilon} \frac{\varepsilon}{k} \nu_T \left( \frac{\partial \bar{U}_i}{\partial x_j} + \frac{\partial \bar{U}_j}{\partial x_i} \right) \frac{\partial \bar{U}_i}{\partial x_j} - C_{2\varepsilon} \frac{\varepsilon^2}{k} \end{aligned} \quad (10)$$

Here,  $\nabla^2$  is the usual Laplacian operator, and the values of the model coefficients  $C_\mu$ ,  $C_\varepsilon$ ,  $C_k$ ,  $C_{1\varepsilon}$  and  $C_{2\varepsilon}$  are determined by comparing the simulation result with experimental data. The model above can be solved easily by numerical techniques, but turns out to be inaccurate especially in flows with separation. Yakhot et. al developed another technique to model the turbulence explicitly as follows:

$$\rho u_i \frac{\partial k}{\partial x_i} = \frac{\partial}{\partial x_i} \left( \left( \mu + \frac{\mu_T}{\sigma_k} \right) \frac{\partial k}{\partial x_i} \right) + \mu_t S^2 - \rho \varepsilon \quad (11)$$

*Convection = Diffusion + Generation + Dissipation*

$$\rho u_i \frac{\partial \varepsilon}{\partial x_i} = \frac{\partial}{\partial x_i} \left( \left( \mu + \frac{\mu_T}{\sigma_\varepsilon} \right) \frac{\partial \varepsilon}{\partial x_i} \right) + C_{1\varepsilon} \frac{\varepsilon}{k} S^2 - \rho C_{2\varepsilon}^* \frac{\varepsilon^2}{k} \quad (12)$$

*Convection = Diffusion + Generation + Destruction*  
where

$$S = (2S_{ij}S_{ij})^{\frac{1}{2}} \quad (13)$$

$$S_{ij} = \frac{1}{2} \left( \frac{\partial u_i}{\partial x_j} + \frac{\partial u_j}{\partial x_i} \right) \quad (14)$$

$$\eta = S \frac{k}{\varepsilon} \quad (15)$$

$$C_{2\varepsilon}^* = C_{2\varepsilon} + \frac{C_\mu \left( 1 - \frac{\eta}{\eta_0} \right)}{1 + \beta \eta^3} \quad (16)$$

$$\mu_T = \rho C_\mu \frac{k^2}{\varepsilon} \quad (17)$$

where  $\mu_T$  is the turbulent viscosity and  $S$  is the mean rate of strain. This model, called the k- $\varepsilon$  RNG model, is similar to the standard k- $\varepsilon$  equations. It adds a term to the dissipation rate equation to represent the correlation between the turbulence dissipation and the mean shear. In addition, there is a differential formula for effective viscosity in the diffusive transport term. The constants are derived explicitly using a statistical technique (except for  $\beta$ ), and their customary values are:  $C_{1\varepsilon}$  1.42,

$\sigma_k = 0.7194$ ,  $\sigma_\varepsilon = 0.7194$ ,  $C_{2\varepsilon} = 1.68$ ,  $C_\mu = 0.0845$ ,  $\eta_0 = 4.38$ , and  $\beta = 0.012$ .

The extra term in the equation improves the performance for separating flow and recirculation regions. Providing many improvements and being an alternative form of the standard model, it is slightly more resource intensive to solve, but the improvements cover wind flows around buildings in an urban setting.

## 2.2. Solving the wind flow model

Since the models that accurately reflect the wind flow are analytically intractable, computational fluid dynamics (CFD) models are solved mainly by numerical techniques. Regardless to the technique used, a successful CFD simulation of the wind in the urban environment depends on three critical points: correct boundary conditions, accurate wind mean profiles and a good mesh quality; since a coarse mesh results in poor output and a very fine mesh will take a long time to converge.

Some early work on wind flow around buildings can be found in [9] and [4]. A more comprehensive study on flow around sets of adjacent tall buildings, possibly with different roof inclinations, was made by Lu *et al.* in [7]. From the various scenarios studied in that research, some of the key conclusions are: (a) for adjacent tall buildings with a narrow gap and a prevailing wind direction along the gap, there is a significant increase in the wind velocity through the gap; (b) higher turbulence (which is detrimental to efficiency of VAWTs) is observed in the layer up to 3m around building edges; (c) for roof mounted turbines, the tallest building in a group of flat-roofed buildings is the ideal choice; however, if the roof-tops are inclined, then the actual configuration of the buildings dictates the ideal choice.

Our interest is in investigating the optimum shape of a channel housing the VAWT. One study aiming at measuring the performance of the wind turbines placed inside tunnels was conducted by Li *et al.* [6]. They mainly conducted a series of wind tunnel experiment simulating the Pearl River tower energy performance according to the local climate data, under different conditions (with or without the surrounding buildings, and with or without the presence of the VAWT in the channel). The main findings were that the power generated was affected by the building orientation, and that a contraction in the shape of the channel resulted in increased wind speeds (and therefore higher power). The latter result corresponds to the knowledge used in design of a traditional venturi. Nevertheless, it has been shown (for example, see [1]), that a venturi (or channel) shape with the highest contraction ratio is not necessarily the best in terms of power output. In all cases of such investigations, wind

tunnel experiments are necessary for validation of the CFD models.

The following sections provide details of our approach, summarized as follows. We build a reduced scale model of a skyscraper with a classic venturi-shaped opening. We will use it to conduct the wind tunnel experiments using wind profiles for a city (in our case, the Hong Kong wind code [2]). Then, using OpenFoam, we build our CFD model based on the RANS equations and applying the RNG k- $\varepsilon$  turbulence model. In this stage, we run the simulation on the reduced scale model of the wind tunnel experiment. The results of this simulation are compared with the wind tunnel measurements in order to validate the developed model. Once its accuracy confirmed, the CFD model is used to simulate the wind speed for different shapes of the channel profile represented by a parametric curve (Bezier). By running the simulation over multiple shapes (generated by varying the control points), we obtain enough data to allow the use of a Design of Experiments technique and a prediction model in order to find the optimal shape that conducts normal winds through the channel.

## 3. Wind tunnel experiments

For our study, we use a building that has a square base 30m $\times$ 30m and a height of 120m. The opening is a circular venturi-shaped tunnel. For the wind tunnel experiment, we use a 1:150 reduced-scale model. The outer circle has a radius of 4.56 cm and the radius at the contraction is 4 cm. The calibrated wind profile presents a wind speed at building height ( $z = 0.8$  m) of  $UH = 10.171$  m/s. We dressed the power law for the wind speed profile to be implemented at the inlet boundary with  $\alpha = 0.11$ . The High Speed Test Section has a cross sectional area of 3m  $\times$  2m. It results in a blockage ratio of 2.66% which is less than 3% as recommended by Tominaga *et al.* [11]. The wind velocity and the turbulence intensity, we calibrate the wind profile inspired by the Hong Kong wind

**Table 1.** Data points defining the theoretical wind profile.

Wind tunnel data points			
Points	Height z(m)	Mean wind speed	Turbulence intensity
1	0.067	7.739	0.134
2	0.133	8.352	0.124
3	0.200	8.733	0.119
4	0.333	9.237	0.113
5	0.360	9.316	0.112
6	0.500	9.659	0.108
7	0.667	9.969	0.104
8	0.800	10.171	0.102
9	1.000	10.424	0.100

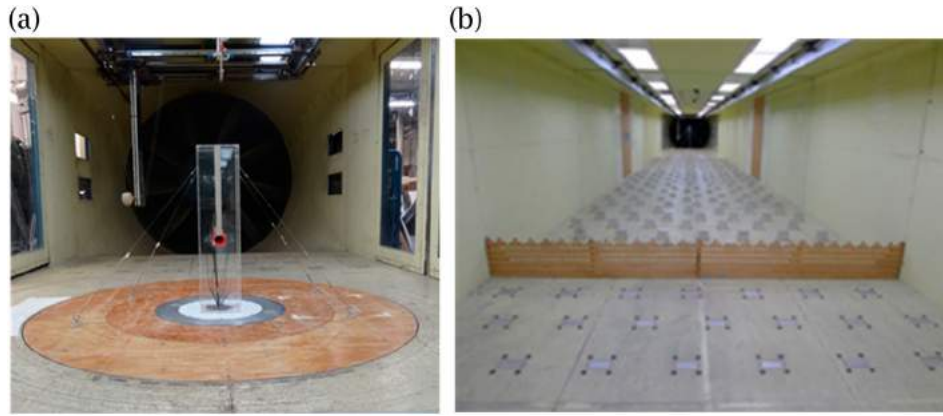


**Figure 2.** (a) The physical scaled model (b) Roughness elements used in wind profile calibration.

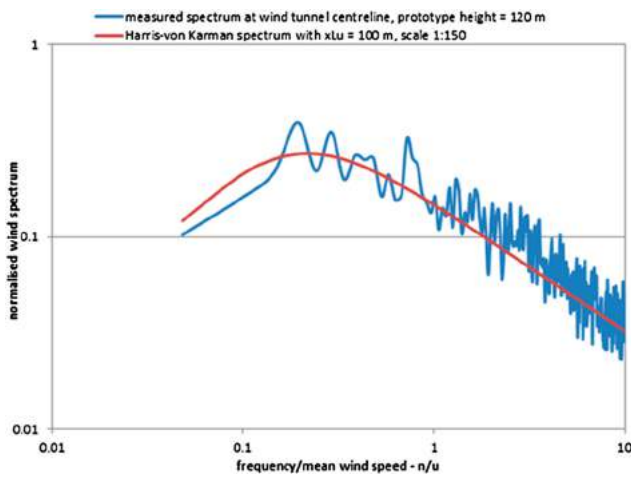


**Figure 3.** Measured spectrum at the wind tunnel Vs. Harris-Von Karman spectrum.

code [2].

$$U(z) = 59.5 * \left(\frac{z}{500}\right)^\alpha \quad (18)$$

$$Iu(z) = 0.1055 * \left(\frac{z}{90}\right)^{-\alpha} \quad (19)$$

We divide the velocity by 5 for our wind tunnel experiments and we keep the same turbulence intensity for the reduced scale model. Our profile is defined by 9 different points. Further, mechanical roughness elements along the wind passage were used to yield a good approximation to the wind profile. Figure 2 shows the setup in the wind tunnel.

Apart from wind velocity and turbulence calibration, we also ensure that we match the wind flow distribution; with the correct settings and parameters, the created dimensionless turbulence and the Von K arm an spectra should match. This is verified by the plot in Figure 3.

The wind speed was measured at five different locations: (i) windward facade at mid-point of the channel;

**Table 2.** Wind tunnel measurements at the critical positions.

Measurement location	Wind speed (m/s)	Turbulence intensity (%)
Measurement, Ang 000p0, T01(F100mm)	5.46074	17.2585
Measurement, Ang 000p0, T02	10.0935	9.09847
Measurement, Ang 000p0, T03	13.9799	10.7288
Measurement, Ang 000p0, T04	11.5012	11.9787
Measurement, Ang 000p0, T05(B100mm)	6.2479	53.2507

(ii) midpoint of the contraction cross-section of the channel; (iii) mid-point of the exit profile of the channel, and (iv, v) two points, each 10cm away from the windward (respectively, leeward) facade of the model and along the axis of the channel. Table 2 shows the measured data for the wind tunnel experiments. Using a characteristic length equal to the width of the building, we obtain a Reynolds number  $Re = \frac{UD}{\nu} \approx 1.8 \times 10^5$  which is in the range of flows around buildings ( $\sim 10^5$ ).

#### 4. CFD simulation

We use an open source CFD solver, OpenFoam, for our simulations. The first step is to generate the mesh. We developed a simple python script to generate the definition for the mesh in a BlockMeshDict file, which is used by the BlockMesh utility in OpenFoam to create a non-uniform graded mesh. The cells in the region of the interest are small, while those further away from the building are larger. Figure 4 shows the top and elevation views of the mesh.

As discussed before, we first create one mesh with a circular profile venturi shape hole in the building to validate the parameters of the simulation with the wind tunnel experimental data. Next, we create a series of test shapes, where the channel is a rectangular profile hole whose height remains constant, but the width varies as per a degree-3 Bezier curve. The control points  $P_1$  and

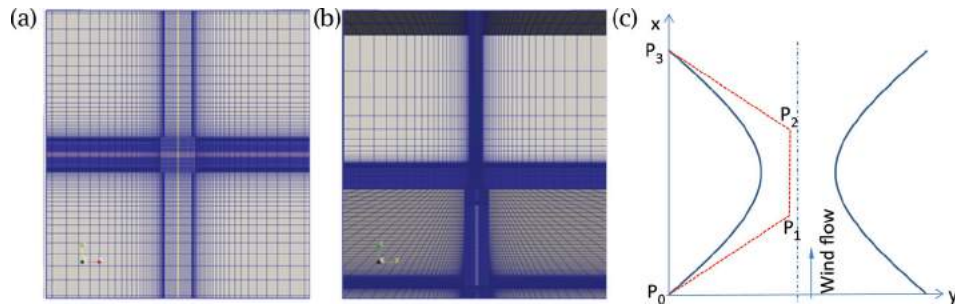


**Figure 4.** (a) Top view and (b) elevation view of the simulation mesh in OpenFoam (c) Horizontal cross-section of channel showing symmetric left- and right profiles; dashed red lines show the control polygon of the Bezier curve defining the left profile.

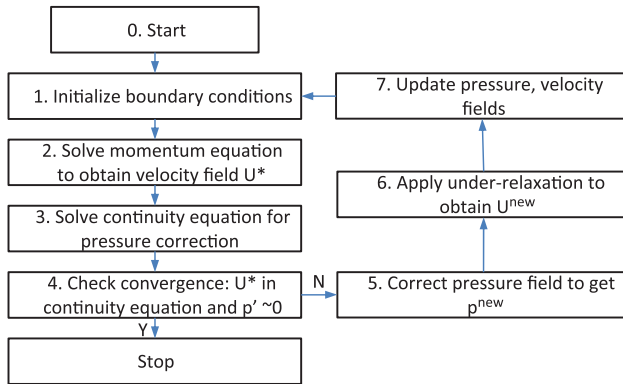


**Figure 5.** Flowchart of the SIMPLE algorithm.

$P_2$  are moved to change the profile shape. As mentioned before, we use the RNG  $k-\varepsilon$  model, with the coefficients as given in the previous section. The finite volume method is used in OpenFOAM, and the initialization process includes the input of the values at every boundary. The Semi-Implicit Method for Pressure Linked Equations (SIMPLE) algorithm, which is a built-in utility in OpenFOAM, was used. We omit the other implementation and tuning details for the computation, except to give the overall flow used by the SIMPLE solver in Figure 5. Table 3 shows that the CFD model results, compared to the wind tunnel data, have an error of less than 5% at the critical positions.

## 5. DOE approach for optimal design of VAWT channels

The shape of the channel in our study was varied by moving the coordinates  $(x_1, y_1)$ ,  $(x_2, y_2)$  of the control points

$P_1$  and  $P_2$ . If we use three different values for each of these four variables, then we potentially have to run  $3^4 = 81$  experiments. Since each simulation takes several hours to run, we decided to run a partial factorial experiment. The results of the 27 runs we executed are shown in Table 4. Figure 6 shows the flow streamlines through two shapes of the channels (runs #3 and #24).

In three runs (19, 20 and 21), we deliberately choose the control points as to check the concavity effect with  $x_1$  smaller than  $x_2$  (5.6). In these runs, the bowl shape effect is checked when compared to the runs 13, 14 and 15. The same contraction ratio is kept in a case by case basis. In other words we will compare 13 vs. 19, 14 vs. 20 and 15 vs. 21. One of the counter-intuitive results of the simulations is that the shape of the opening before the neck-point is less significant than we had initially expected. Its impact on the speed at the contraction point is relatively less significant. Furthermore, even the shape, i.e. the concavity or convexity of the initial segments of the tunnel profile does not have a significant effect on the maximum velocity at the contraction. Indeed, the difference in the maximum velocity reached at mid-height between the two configurations (concavity vs. convexity) does not exceed 4%, 3% and 1% for the three comparisons. The output is displayed in Figure 7. Simple analysis of the results indicates that contraction is a significant factor. Secondly, at a fixed value of  $y_1$ , higher values for  $y_2$  have high impact on the maximum velocity. Thirdly, by looking at the turbulence values at maximum contraction, it is beneficial to locate the point of maximum contraction far from the windward façade.

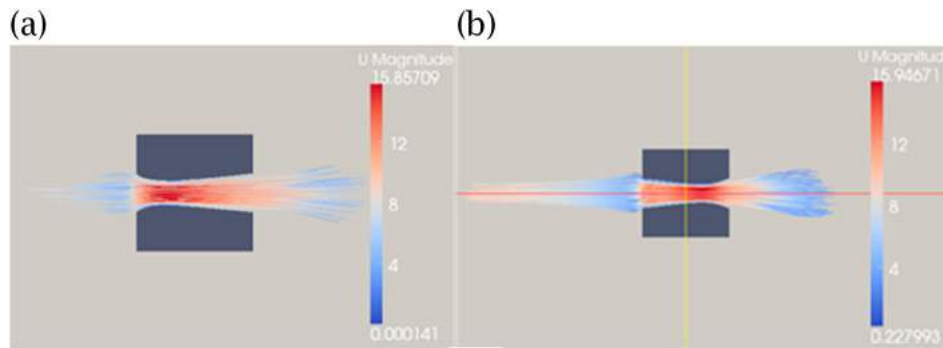
Finally, we use a statistical interpolation technique, Kriging (see [8] for the theory), to search for the optimum

**Table 3.** Comparison between the wind tunnel measurements and CFD simulation results.

Measurement location	Wind tunnel U (m/s)	CFD Model U(m/s)	Error
Measurement, Ang 000p0, T01(F100mm)	5.46074	6.00248	9.92%
<b>Measurement, Ang 000p0, T02</b>	<b>10.0935</b>	<b>9.57324</b>	<b>-5.15%</b>
<b>Measurement, Ang 000p0, T03</b>	<b>13.9799</b>	<b>13.6155</b>	<b>-2.61%</b>
<b>Measurement, Ang 000p0, T04</b>	<b>11.5012</b>	<b>11.1087</b>	<b>-3.41%</b>
Measurement, Ang 000p0,T05(B100mm)	6.2479	5.63031	-9.88%

**Table 4.** Settings and results for the DoE experimental runs.

Run	A	B	C	D	x1	x2	y1	y2	Maximum velocity	Contraction location	TI (%)
1	0	0	0	0	0.02	0.05	0.01	0.01	13.6943	0.052	15.06%
2	0	0	1	1	0.02	0.05	0.013333	0.013333	14.5711	0.052	14.89%
3	0	0	2	2	0.02	0.05	0.016667	0.016667	15.757	0.052	14.24%
4	0	1	0	1	0.02	0.15	0.01	0.013333	14.4025	0.097	13.03%
5	0	1	1	2	0.02	0.15	0.013333	0.016667	15.2674	0.097	12.52%
6	0	1	2	0	0.02	0.15	0.016667	0.01	14.6372	0.082	12.84%
7	0	2	0	2	0.02	0.18	0.01	0.016667	14.586	0.109	12.18%
8	0	2	1	0	0.02	0.18	0.013333	0.01	14.1509	0.091	13.15%
9	0	2	2	1	0.02	0.18	0.016667	0.013333	15.465	0.091	12.40%
10	1	0	0	1	0.05	0.05	0.01	0.013333	14.1149	0.07	14.66%
11	1	0	1	2	0.05	0.05	0.013333	0.016667	15.3447	0.07	13.50%
12	1	0	2	0	0.05	0.05	0.016667	0.01	14.7936	0.061	13.93%
13	1	1	0	2	0.05	0.15	0.01	0.016667	14.8352	0.109	12.34%
14	1	1	1	0	0.05	0.15	0.013333	0.01	14.3007	0.091	14.01%
15	1	1	2	1	0.05	0.15	0.016667	0.013333	15.1128	0.094	12.58%
16	1	2	0	0	0.05	0.18	0.01	0.01	13.7272	0.103	13.34%
17	1	2	1	1	0.05	0.18	0.013333	0.013333	14.6938	0.118	11.98%
18	1	2	2	2	0.05	0.18	0.016667	0.016667	15.6291	0.118	11.32%
19	2	0	0	2	0.15	0.05	0.01	0.016667	14.2881	0.109	12.50%
20	2	0	1	0	0.15	0.05	0.013333	0.01	13.918	0.097	13.31%
21	2	0	2	1	0.15	0.05	0.016667	0.013333	15.0351	0.097	12.83%
22	2	1	0	0	0.15	0.15	0.01	0.01	13.5455	0.13	12.47%
23	2	1	1	1	0.15	0.15	0.013333	0.013333	14.6984	0.136	11.40%
24	2	1	2	2	0.15	0.15	0.016667	0.016667	15.7904	0.139	10.84%
25	2	2	0	1	0.15	0.18	0.01	0.013333	13.8489	0.148	11.77%
26	2	2	1	2	0.15	0.18	0.013333	0.016667	15.1455	0.148	10.97%
27	2	2	2	0	0.15	0.18	0.016667	0.01	14.7088	0.136	11.47%

**Figure 6.** Horizontal cross-section at the middle of the channel in (a) run #3, and (b) run #24.

configuration that interpolates the discrete data set generated from the 27 runs. Expressing the  $i$ -th design configuration as  $x_i = (x_{1i}, x_{2i}, y_{1i}, y_{2i})$ ,  $i = 1, 27$ , we can write the basic Kriging model as:

$$y(x_i) = \mu + z(x_i) \quad (20)$$

Here,  $z(x)$  is a Gaussian process with zero mean and variance  $\sigma^2$ , and correlation function:

$$r(\theta, s, t) = \text{Corr}(z(s), z(t)) = \exp \left\{ - \sum_{k=1}^4 \theta_k |s_k - t_k|^2 \right\} \quad (21)$$

The general Kriging model is written as follows:

$$y(x) = \sum_{j=0}^L \beta_j B_j(x) + z(x) \quad (22)$$

where  $\{B_j(x), j = 1, \dots, L\}$  is a chosen basis over the experimental domain;  $\beta = (\beta_0, \dots, \beta_L)'$ ,  $y = (y_1, y_2, \dots, y_n)'$ , and  $b(x) = (B_0(x), \dots, B_L(x))'$  with covariance functions:

$$B = \begin{bmatrix} B_0(x_1) & \dots & B_L(x_1) \\ \vdots & \ddots & \vdots \\ B_0(x_n) & \dots & B_L(x_n) \end{bmatrix}$$

$Z$  can be written as  $(z_1, z_2)$  where  $z_1$  is the configuration we want to estimate and  $z_2$  the set of errors of the experimental data in hand:  $z_2$  is  $n$  dimensional and  $z_1$  is one-dimensional. Indeed, it is a conditional expected value:

$$\hat{z}_1 = E(z_1 | z_2) = \sum_{12} \sum_{22} z_2 \quad (23)$$

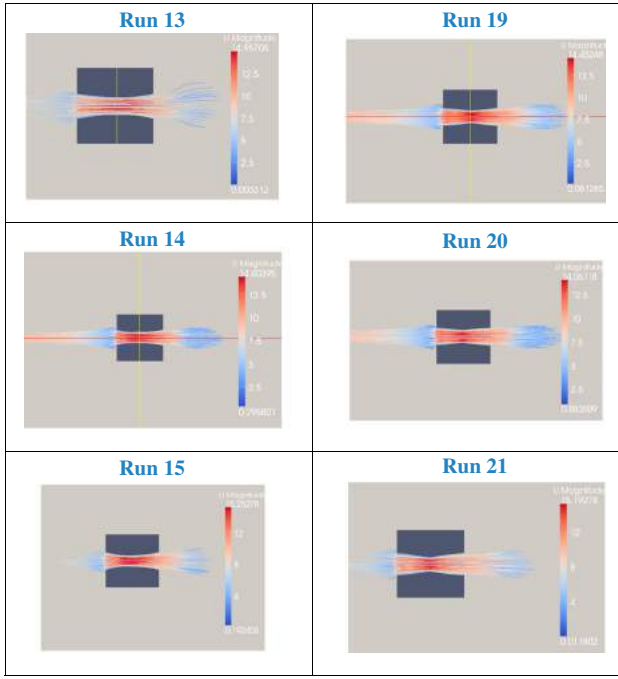


**Figure 7.** Streamlines through the tunnel in runs (a) 13; (b) 14; (c) 15; (d) 19; (e) 20 and (f) 21.

With  $\sum_{12} = cov(z_1, z_2)$  and  $\sum_{22} = cov(z_2)$ , and  $z(x^*) = y(x^*) - \sum_{j=1}^L \beta_j B_j(x^*)$ . As  $(z(x^*), z(x_1), z(x_2), \dots, z(x_n)) \sim N_{n+1}(0, \sigma^2)$ , we obtain  $z(x^*)$  using (23). Then, we insert it in the following equation to get  $y(x^*)$ .

$$\hat{y}(x) = b(x)\hat{\beta} + r'(x)R^{-1}(\theta)(y - B\hat{\beta}) \quad (24)$$

$$MSE = \sigma^2 \left[ 1 - (b'(x), r'(x)) \begin{pmatrix} 0 & B' \\ B & R^{-1}(\theta) \end{pmatrix} \begin{pmatrix} b(x) \\ r(x) \end{pmatrix} \right]$$

From the normality assumption of the Gaussian Kriging model, the density of  $y$  is:

$$(2\pi\sigma^2)^{-n/2} |R(\theta)|^{-1/2} \exp\left(-\frac{1}{2\sigma^2} (y - B\hat{\beta})' R^{-1}(\theta) (y - B\hat{\beta})\right) \quad (25)$$

Corresponding to which the log likelihood can be written as:

$$l(\beta, \sigma^2, \theta) = -n/2 \log(\sigma^2) - 1/2 \log |R(\theta)| - \frac{1}{2\sigma^2} (y - B\hat{\beta})' R^{-1}(\theta) (y - B\hat{\beta}) \quad (26)$$

This allows one to estimate  $\beta$  and  $\sigma^2$ ,  $\theta$  separately and iteratively. For a given  $\theta$ , the maximum likelihood estimate of  $\beta$ , is given after the minimization with respect to  $\beta$  of  $(y - B\hat{\beta})' R^{-1}(\theta) (y - B\hat{\beta})$ :

$$\hat{\beta}_{MLE} = (B'R^{-1}(\theta)B)^{-1} B'R^{-1}(\theta)y \quad (27)$$

We use an iterative procedure using the statistical package R to solve this. The solution was also tested using a

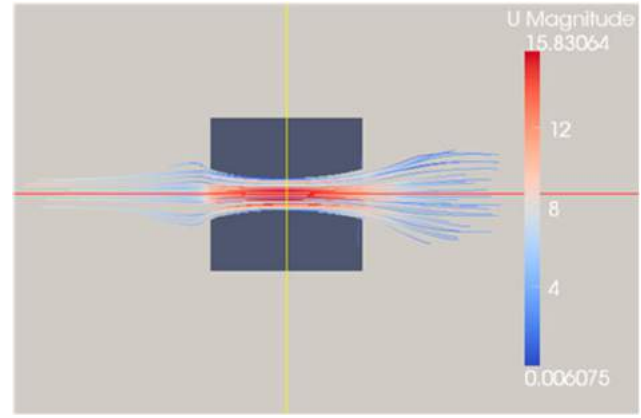


**Figure 8.** Streamlines in the optimal configuration given by the Kriging model.

simple leave-out-one cross-validation process. The optimum solution based on this interpolation is obtained as  $x = (x_1, x_2, y_1, y_2) = (0.0344, 0.1511, 0.0167, 0.0167)$ . That means a contraction at its maximum and located at 0.945m from the building windward surface upstream, and with a predicted a maximum velocity of 15.96 m/s. This was verified by another run with these parameters in OpenFoam (see Figure 8).

## 6. Conclusions

We conclude the paper by summarizing our main contribution, which is the development of a systematic approach using a combination of parametric design, Design of experiments and machine learning tools. The approach is verified by testing on an example building with a simple rectangular channel whose vertical walls are bounded by parametric surfaces and which can house a VAWT. We show that the design does have significant impact on the maximum wind velocity at the contraction point, and therefore on the VAWT output.

## Acknowledgements

Part of this research was funded by GRF grant #613312, and supported by the Wind tunnel facility in HKUST.

## ORCID

Ajay Joneja  <http://orcid.org/0000-0002-6797-1253>

Tim K.T. Tse  <http://orcid.org/0000-0002-9678-1037>

## References

- [1] Blocken, B.; van Hooff, T.; Aanen, L.; Bronsema, B.: Computational analysis of the performance of a venturi-shaped roof for natural ventilation: venturi-effect versus

- wind-blocking effect, *Computers & Fluids*, 48, 2011, 202–213. <http://doi.org/10.1016/j.compfluid.2011.04.012>
- [2] Building Department: “Code of practice on wind effects in hong kong,” The Government of the Hong Kong Special Administrative Region, 2004.
- [3] Hanjalic, K.; Launder, B.: A Reynolds stress model of turbulence and its application to thin shear flows, *Journal of Fluid Mechanics*, 52, 1972, 609–638. <https://doi.org/10.1017/S002211207200268X>
- [4] Heath, M. A.; Walshe, J. D.; Watson, S. J.: Estimating the potential yield of small building-mounted wind turbines, *Wind Energy*, 10, 2007, 271–287. <http://doi.org/10.1002/we.222>
- [5] Kolmogorov, A. N.: The local structure of turbulence in incompressible viscous fluid for very large Reynolds numbers, *Doklady Akademili Nauk SSSR*, 1941, 299–303.
- [6] Li, Q.; Chen, F.; Li, Y.; Lee, Y.: Implementing wind turbines in a tall building for power generation: A study of wind loads and wind speed amplifications, *Journal of Wind Engineering and Industrial Aerodynamics*, 116, 2013, 70–82. <http://doi.org/10.1016/j.jweia.2013.03.004>
- [7] Lu, L.; Ip, K. Y.: Investigation on the feasibility and enhancement methods of wind power utilization in high-rise buildings of Hong Kong, *Renewable and Sustainable Energy Reviews*, 13, 2009, 450–461. <http://doi.org/10.1016/j.rser.2007.11.013>
- [8] Matheron, G.: Principles of geostatistics, *Economic Geology*, 58, 1963, 1246–1266. <http://doi.org/10.2113/gsecongeo.58.8.1246>
- [9] Mertens, S.: The energy yield of roof mounted wind turbines, *Wind Engineering*, 27, 2003, 507–518.
- [10] Reynolds, O.: On the dynamical theory of incompressible viscous fluids and the determination of the criterion, *Philosophical Transactions of the Royal Society of London, A*, 1895, 123–164. <http://doi.org/10.1098/rsta.1895.0004>
- [11] Tominaga, Y.; Mochida, A.; Yoshie, R.; Kataoka, H.; Nozu, T.; Yoshikawa, M.; Shirasawa, T.: AIJ guidelines for practical applications of CFD to pedestrian wind environment around buildings, *Journal of Wind Engineering and Industrial Aerodynamics*, 96, 2008, 1749–1761. <http://doi.org/10.1016/j.jweia.2008.02.058>
- [12] [www.wikipedia.org](http://www.wikipedia.org): Pearl River Tower